JACS
JOURNAL OF THE AMERICAN CHEMICAL SOCIETY
Article
pubs.acs.org/JACS

Far-Red Fluorescence Probe for Monitoring Singlet Oxygen during Photodynamic Therapy

Sooyeon Kim, Takashi Tachikawa, Mamoru Fujitsuka, and Tetsuro Majima*

The Institute of Scientific and Industrial Research (SANKEN), Osaka University, Mihogaoka 8-1, Osaka, Ibaraki 567-0047, Japan

Supporting Information

ABSTRACT: Singlet oxygen ($^1O_2$), molecular oxygen in the lowest excited state, has a critical role in the cell-killing mechanism of photodynamic therapy (PDT). Although $^1O_2$ phosphorescence measurement has been mainly used to monitor $^1O_2$ formation during PDT, its intensity is far insufficient to obtain two-dimensional images of intracellular $^1O_2$ with the subcellular spatial resolution using the currently available near-IR detector. Here, we propose a new far-red fluorescence probe of $^1O_2$, namely, Si-DMA, composed of silicon-containing rhodamine and anthracene moieties as a chromophore and a $^1O_2$ reactive site, respectively. In the presence of $^1O_2$, fluorescence of Si-DMA increases 17 times due to endoperoxide formation at the anthracene moiety. With the advantage of negligible self-oxidation by photoirradiation (Φ_Δ < 0.02) and selective mitochondrial localization, Si-DMA is particularly suitable for imaging $^1O_2$ during PDT. Among three different intracellular photosensitizers (Sens), Si-DMA could selectively detect the $^1O_2$ that is generated by 5-aminolevulinic acid-derived protoporphyrin IX, colocalized with Si-DMA in mitochondria. On the other hand, mitochondria-targeted KillerRed and lysosomal porphyrins could not induce fluorescence change of Si-DMA. This surprising selectivity of Si-DMA response depending on the Sens localization and photosensitization mechanism is caused by a limited intracellular $^1O_2$ diffusion distance (~300 nm) and negligible generation of $^1O_2$ by type-I Sens, respectively. For the first time, we successfully visualized $^1O_2$ generated during PDT with a spatial resolution of a single mitochondrial tubule.

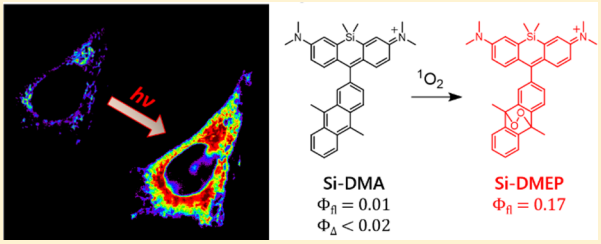

INTRODUCTION

Singlet oxygen ($^1O_2$) is molecular oxygen in the lowest excited state.[1] In biological and medical studies, $^1O_2$ is of a particular importance because of its key role in photodynamic therapy (PDT), an emerging anticancer treatment using photoirradiation and photosensitizers (Sens).[2] In PDT, $^1O_2$ is the first molecule immediately generated after photoirradiation in the aerobic condition, resulting in direct oxidation of nearby biomolecules, shutdown of the vascular system, and finally inflammation or immune reaction to tumor tissue.[3] Hence, investigating the formation and diffusion dynamics of $^1O_2$ is highly necessary to understand anticancer mechanisms of PDT at the molecular level.

Cytotoxic mechanisms of Sens in PDT can be explained as type-I and type-II.[1,2] Type-II photosensitization includes all kinds of reactions where the excited Sens is quenched by a collision with oxygen in the ground state ($^3O_2$). Meanwhile, in type-I photosensitization, adjacent molecules (except $^3O_2$) quench the excited Sens often through electron transfer. Upon photoirradiation of injected photosensitizers, a majority of $^1O_2$ is produced via triplet−triplet intermolecular energy transfer (TTEnT) from Sens in the triplet excited state (^{3}Sens*) to $^3O_2$ (eq 1).

$$^3\text{Sens}^* + {}^3O_2 \rightarrow {}^1\text{Sens} + {}^1O_2 \quad (1)$$

This is a typical reaction of $^1O_2$ formation via type-II photosensitization. On the other hand, it is notable that the superoxide anion can be generated by either type-I, type-II, or secondary biological processes after photoirradiation, such as mitochondrial damage. As summarized in previous reviews,[2,4−6] the superoxide anion often acts as a "primary" reactive oxygen species (ROS) because they can be further converted into other ROS such as H_2O_2 and $^1O_2$ through various biological reactions.

To detect $^1O_2$, phosphorescence measurement has been generally used in PDT.[1,7,8] From time-resolved phosphorescence measurement, intracellular $^1O_2$ lifetime (τ_Δ) is found to be varied from a few tens of nanoseconds to 3 μs, depending on the experimental conditions.[2,7,9] Undoubtedly, monitoring $^1O_2$ with its luminescence provides the most direct information on $^1O_2$ formation and further behaviors. Unfortunately, however, the intensity of phosphorescence is typically much weaker than that of fluorescence. In addition, to obtain time trajectories of $^1O_2$ with good signal-to-noise ratio, the exchange of intracellular liquid from H_2O to D_2O is mostly required. Thus, real-time mapping (e.g., subsecond acquisition time) of $^1O_2$ formation at the subcellular spatial resolution is extremely challenging using the currently available near-IR detector and under physiological conditions.[10,11] Considering the current problems, the fluorescence detection of $^1O_2$ is ultimately required to trace $^1O_2$ formation and its dynamics at the

Received: April 29, 2014
Published: July 30, 2014

   dx.doi.org/10.1021/ja504279r | J. Am. Chem. Soc. 2014, 136, 11707−11715

subcellular level under physiological conditions (i.e., H_2O-based culture media).

Despite continuous efforts on the development of a fluorescent probe for $^1O_2$ detection (see examples in Supporting Information Figure S1),[12−15] merely a few cases enabled imaging $^1O_2$ in living cells.[16−20] Moreover, Singlet Oxygen Sensor Green (SOSG), a widely used commercial $^1O_2$ probe, exhibits several critical weak points in live cell imaging: self-oxidation upon photoirradiation, cell impermeability (or nonspecific staining at the relatively high incubating concentration; see Figure S2 and ref 21), and a necessity of green excitation (λ_{abs} = 508 nm) where a cell autofluorescence signal is induced.[21,22] To the best of our knowledge, only Song et al.[16] and Dai et al.[17] have succeeded in monitoring intracellular $^1O_2$ produced during photoirradiation of Sens using the fluorescent probe based on europium complexes. Surprisingly, however, there has been no adequate $^1O_2$ fluorescence probe to monitor intracellular $^1O_2$ during PDT at the subcellular level. The drawbacks of SOSG and lack of a suitable and successful organic probe for $^1O_2$ mapping have inspired us to develop a new far-red fluorescent probe for the $^1O_2$ detection.

In this study, we have synthesized a far-red fluorescent probe of $^1O_2$, composed of 9,10-dimethylanthracene (DMA) and silicon-containing rhodamine (Si-rhodamine) moieties, namely, Si-DMA (Figure 1). Recently, Si-rhodamine has been actively

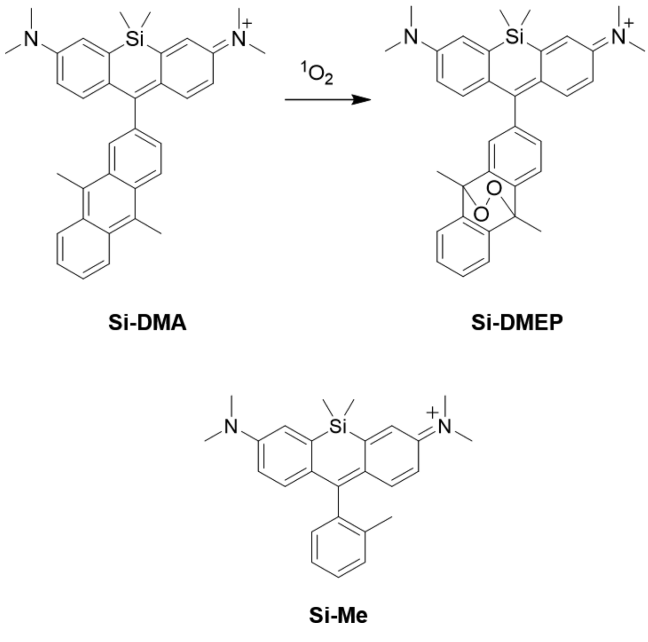

Figure 1. Chemical structures of Si-DMA, its peroxidized product (Si-DMEP), and Si-Me.

applied for the detection of various biological substances[23−26] and super-resolution imaging both in vitro and in vivo.[27] In light of the previous works, we affirmed that Si-rhodamine is a promising far-red chromophore for the intracellular $^1O_2$ mapping. Here, Si-rhodamine is found to exhibit 3 times lower quantum yield of $^1O_2$ generation (Φ_Δ) than that of 2,7-dichlorofluorescein, a chromophore of SOSG. Furthermore, Si-DMA can selectively reside in mitochondria and provide an instantaneous response to intracelluar $^1O_2$. Compared to the previously reported intracellular $^1O_2$ probes,[16−19] Si-DMA shows outstanding results to visualize intracellular $^1O_2$ in real-time and to distinguish different localizations of Sens and photosensitization mechanisms.

EXPERIMENTAL SECTION

Materials. All chemical reagents and solvents used for the synthesis were purchased from Sigma-Aldrich Chemical Co., Tokyo Chemical Industries, Nacalai Tesque, and Wako Pure Chemical, and used as received. 2-Methylbenzene-substituted Si-rhodamine (Si-Me, Figure 1) was synthesized according to the previous report by Koide et al.,[23] and Si-DMA was synthesized as described in Supporting Information. Si-DMA and Si-Me were stored in dimethyl sulfoxide (DMSO) at −20 °C in the dark. We chose the following Sens for living cell experiments: 5-aminolevulinic acid (5-ALA, Sigma-Aldrich), a precursor of heme, and tetra-(*N*-methyl-4-pyridyl)porphyrin (TMPyP4, Tokyo Chemical Industries). SOSG, CellROX Green, MitoTracker Green FM, and Dextran 10000 MW labeled by Alexa Fluor 488 or Alexa Fluor 647 (A488- and A647-dextran, respectively) were purchased from Molecular Probes and used for $^1O_2$ and ROS detection, mitochondrial and lysosomal markers, respectively.

Ex Vivo Steady-State Measurements. Without a notation, all bulk spectroscopic measurements were performed in methanol at the spectroscopic grade or pH 7.5 phosphate buffered saline (PBS) solution without Ca and Mg (both purchased from Nacalai Tesque). Ground-state absorption and fluorescence emission spectra were measured using a Shimadzu UV-3100 and Horiba FluoroMax-4, respectively. Bulk irradiation was performed using a xenon source (LAX-C100, Asahi Spectra) and band-pass filter (BA510-550, Olympus).

Time-Resolved Phosphorescence Measurement. The samples of Rose Bengal and Si-Me were prepared in 1:9 DMSO/MeOH solution in a 1 × 1 × 4 cm^3 quartz cell. The second-harmonic oscillation (532 nm, 4 ns fwhm, 5.0 mJ cm^{-2} $pulse^{-1}$) from a Q-switched Nd:YAG laser (Continuum, Surelite II-10) was used for the excitation light. The photoinduced luminescence from the sample cell was collected with quartz lenses, passed through a monochromator, and then introduced into a near-IR photomultiplier tube module (Hamamatsu Photonics, H10330A-75). After being amplified by a 350 MHz amplifier unit (Stanford Research, SR445A), the output of the photomultiplier was sent to a gated photon counter (Stanford Research, SR400) under direct control from a PC via the GPIB interface. To measure the lifetime of $^1O_2$, the signals were accumulated (five repetitions) by changing the delay time from 0 to 50 μs with a gate width of 1.0 μs.

Cells and Cell Culture. HeLa cells and RAW 264.7 macrophages were kindly provided by the RIKEN BRC through the National Bio-Resource Project of the MEXT, Japan, and Prof. Tsuyoshi Nishi (SANKEN, Osaka University), respectively. Without a notation, cell experiments carried out in this study were performed using HeLa cells. HeLa cells and RAW 264.7 macrophages were cultivated in Dulbecco's modified Eagle medium (D6429, Sigma) supplemented with 10% fetal bovine serum (10099-141, Gibco) at 37 °C in a humidified incubator under 5% CO_2.

Live Cell Imaging. To monitor fluorescence increase of Si-DMA during photoirradiation of Sens, an Olympus IX81 inverted fluorescence microscope and a 640 nm CW laser (Coherent) were used to irradiate Sens and monitor the probe simultaneously. A 35 mm μ-dish with a glass bottom (ibidi) with HeLa cells was excited through an oil objective (Olympus, PlanApo 100×/1.40 oil). The emission image was collected with the same objective and recorded by an EMCCD camera (Roper Scientific, Evolve 512) through a dichroic beamsplitter (Semrock, Di02-R635) and a band-pass filter (Chroma, HQ690/70). During data acquisition, the same environment as an incubator (37 °C and 5% CO_2) was maintained using a Chamlide TC (Live Cell Instrument). Pseudocolor fluorescence images were prepared by reprocessing the obtained movie file using OriginPro 9.1 (OriginLab) and ImageJ.

To confirm the localization of dyes, in particular, cellular organelles, an objective scanning confocal microscope (PicoQuant, MicroTime 200) coupled with an Olympus IX71 inverted fluorescence microscope

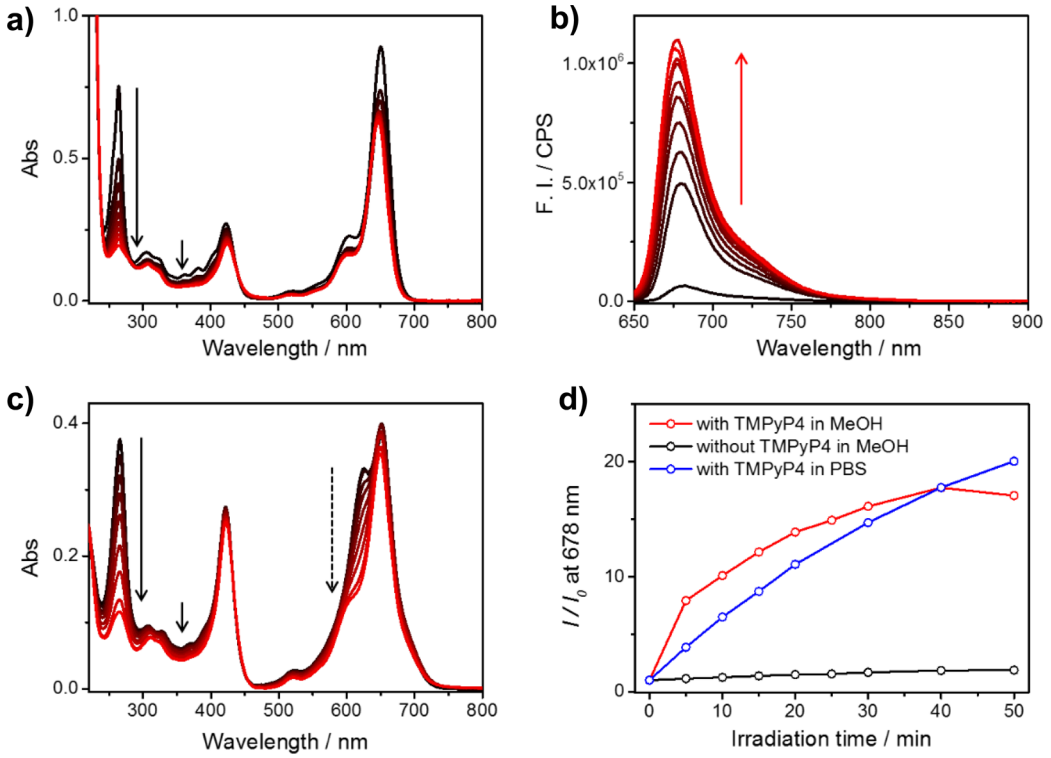

Figure 2. Absorbance and fluorescence changes of Si-DMA in methanol (a,b) and in PBS solution (c) upon photoirradiation of codissolved TMPyP4 for 50 min (black to red). Black arrows in (a,c) indicate absorbance changes due to peroxidation of DMA (bold lines) and dissociation of H-aggregates (dashed lines), while a red arrow in (b) shows fluorescence increase during 50 min irradiation. (d) Si-DMA fluorescence increase during 50 min photoirradiation. [Si-DMA] = 50 μM, [TMPyP4] = 5 μM, and 510−550 nm irradiation at 0.07 W cm^{-2} with magnetic stirring was used for $^1O_2$ formation.

was used. An 8-well μ-slide (ibidi) with HeLa cells was excited at two wavelengths, 405/640 nm or 485/640 nm, using a pulsed laser (PicoQuant) controlled by a PDL-800B driver (PicoQuant) through an oil objective (Olympus, UPlanSAPo 100x/1.40 oil/0.17/FN26.5). Subsequently, the emission was collected with the same objective and detected by a single photon avalanche photodiode (Micro Photon Devices, PDM 50CT and 100CT) through a beam splitter (90% transmission, 10% reflection), suitable band-pass filters, and 75 μm pinhole for spatial filtering to reject out-of-focus signals. Two images for green and red channels were further processed to obtain a merged image using OriginPro 9.1 (OriginLab) and ImageJ.

RESULTS AND DISCUSSION

Synthesis and Optical Properties of Si-DMA. As proposed by Nagano et al.[23] and Johnsson et al.,[27] we first synthesized Si-containing xanthone, and then connected it to 2-bromo-9,10-dimethylanthracene, which is a reactive site for $^1O_2$, resulting in Si-DMA (19% yield). $^1O_2$-induced conversion of Si-DMA to Si-DMEP is illustrated in Figure 1. Detailed synthesis description and characterization can be found in Supporting Information.

Figure 2 shows time-dependent changes in absorbance and fluorescence of Si-DMA upon photoirradiation of coincubated TMPyP4. In the absence of $^1O_2$, the excited Si-rhodamine is quenched by photoinduced electron transfer (PET) from DMA, resulting in dim fluorescence (Φ_{fl} = 0.01 in methanol). Polarity-dependent fluorescence quenching of Si-DMA supports that Si-DMA is indeed deactivated by PET (Figure S3). This intramolecular PET and subsequent charge recombination process in Si-DMA are considered to be similar to the previously reported xanthene−anthracene dyads.[22,28] Furthermore, Si-DMA converts into bright form (Si-DMEP, Φ_{fl} = 0.17 in methanol) by reacting with $^1O_2$ and forming endoperoxide on the center ring of DMA because PET from DMA to Si-rhodamine is prohibited (Figure 1). Approximately, 18-fold increase in fluorescence was observed in MeOH (Figure 2b,d, red), accompanying a disappearance of anthracene absorbance (black arrows, Figure 2a). Similar spectral changes were observed when $^1O_2$ was induced by a chemical catalyst (Figure S4). In addition, it has been reported that some anthracene derivatives, such as arylanthracene and alkynylanthracene, undergo a reversible reaction with $^1O_2$ upon increasing temperature, that is, a formation of endoperoxide and release of O_2.[29] Nonetheless, the DMA moiety in Si-DMA does not release O_2 after endoperoxidation but is probably prone to be decomposed at temperatures above 70 °C, which is much greater than that at physiological conditions.[21]

Interestingly, Si-DMA is found to form H-aggregates in the aqueous solution (Figure 2c). This is because substituting an anthracene moiety reduces the hydrophilicity of Si-DMA as compared to Si-Me, which is a monomer in PBS solution at the same concentration (5 μM). A blue-shifted absorption peak at 625 nm is clear evidence to indicate the H-aggregates of rhodamine chromophores.[30−32] This blue-shifted shoulder gradually decreases as Si-DMEP forms (Figure 2c, red arrow), implying that endoperoxide formation at the anthracene ring disrupts a stacking of rhodamine fluorophores. In Figure 2d, the slower rate of Si-DMEP formation in the case of H-aggregates compared to that of monomeric Si-DMA is presumably caused by (1) a decrease in the absolute chromophore concentration due to the aggregate formation and (2) necessity of aggregate dissociation by (or for) reacting with $^1O_2$. A similar result is also obtained in the presence of

dx.doi.org/10.1021/ja504279r | J. Am. Chem. Soc. 2014, 136, 11707−11715

chemically prepared $^1O_2$ (Figure S5). Furthermore, a larger fluorescence increment observed in PBS solution (22-fold) than that in MeOH (18-fold) is probably due to additional fluorescence quenching upon H-aggregate formation before photoirradiation. Overall, both monomeric and H-aggregates of Si-DMA can react to $^1O_2$, while Si-DMEP does not favor the aggregate formation due to a loss of anthracene planarity.

Evaluations of Si-DMA as a $^1O_2$ Probe. Si-DMA is tested to confirm whether it can respond to $^1O_2$ quantitatively and selectively without self-oxidation of the dye. First, both Si-DMA monomer and H-aggregates show linear fluorescence increase versus [$^1O_2$] generated by $NaClO/H_2O_2$ (Figure S5). Furthermore, Si-DMA exhibits a good selectivity toward $^1O_2$ out of other ROS, which agrees with the previous anthracene-based $^1O_2$ probes (Figure 3).[12,13,16] In addition, no significant fluorescence decrease was observed in various ROS solutions, indicating chromophore stability of Si-DMA against ROS.

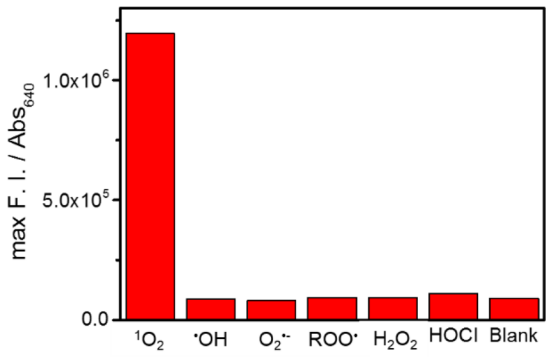

Figure 3. Selectivity of Si-DMA toward $^1O_2$ among other ROS. Maximum fluorescence intensity divided by the absorbance at 640 nm was compared. [Si-DMA] = 5 μM and [ROS] = 10 mM in 1:1 MeOH/PBS solution, stirred for 10 min.

As briefly mentioned earlier, one critical weak point of SOSG is its non-negligible $^1O_2$ generation due to the excitation of the chromophore moiety.[22] Even though most of the SOSG molecules are deactivated via ultrafast intramolecular PET (k_{PET} = 9.7 × 10^{11} s^{-1}), trivial impurities of initially bright SOSG, such as nonsubstituted fluorescein (~0.3%)[33] or peroxidized SOSG molecules, cannot be deactivated via PET and are in charge of $^1O_2$ generation upon continuous photoirradiation.[21,22,33] To observe $^1O_2$ produced during PDT that often requires prolonged photoirradiation from a few minutes to hours, self-oxidation of the dye by light excitation should be avoided. In order to confirm that Si-rhodamine is an appropriate chromophore as a $^1O_2$ probe, Φ_Δ of Si-Me was determined using time-resolved phosphorescence measurement (Figure 4). Using Rose Bengal as a reference (Φ_Δ = 0.76 in MeOH),[34] Φ_Δ of Si-Me is approximately 0.02. This value is considered to reflect the possible maximum Φ_Δ of Si-DMA and Si-DMEP when deactivation pathways via PET is completely blocked. Furthermore, Φ_Δ of Si-Me is 3 times smaller than that of 2,7-dichlorofluorescein, a fluorophore of SOSG (Φ_Δ = 0.06).[22]

Finally, Si-DMA is considered to be fairly photostable, as shown in Figure 2d (black). During 50 min irradiation, no photobleaching is observed in the absence of photosensitizer. In addition, this photostability is maintained when Si-DMA is introduced to HeLa cells (Figure S6). This result is in accordance with the previous study on Si-rhodamine.[24]

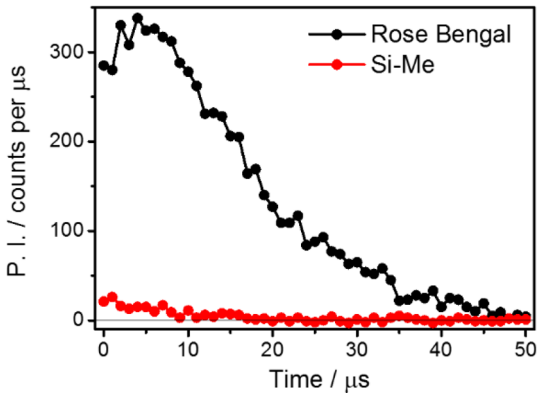

Figure 4. Time profiles of $^1O_2$ phosphorescence intensity (P.I.) of Rose Bengal (black) and Si-Me (red) observed at 1280 nm (λ_{ex} = 532 nm at 5.0 mJ cm^{-2} $pulse^{-1}$) in 1:9 DMSO/MeOH solution. Both samples were prepared to have the same absorbance of 0.5 at 532 nm (path length = 1 cm). [Rose Bengal] = 21.5 μM and [Si-Me] = 250 μM.

Mitochondrial Localization of Si-DMA. Positive net charge of a dye, such as that of rhodamine 123 (R123)[35,36] and lipophilic cyanine cation, JC-1,[37,38] facilitates its mitochondrial accumulation due to mitochondrial membrane potential.[39] Here, we found that Si-DMA can reside in mitochondria with high selectivity (Figure 5). The long, thin, and branched fibrillar

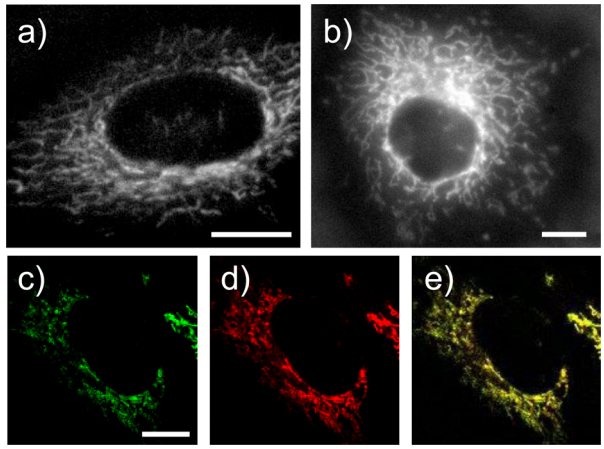

Figure 5. HeLa cells stained with [Si-DMA] = (a) 20 and (b) 100 nM for 1 h. (c–e) Colocalization test of Si-DMA in mitochondria. (c) MitoTracker Green and (d) [Si-DMA] = 100 nM. Clear colocalizations of two dyes are observed in the merged image (e). Intensities of each image have been adjusted to obtain a clear picture. Scale bar = 10 μm.

fluorescence image of Si-DMA clearly proves its selective localization in mitochondria.[40] In addition, it does not have a strong preference to reside in mitochondria around the nucleus or edge of the cell, different from 5-ALA-derived PpIX (discussed later). On the other hand, concentrations higher than 1 μM seem to result in nonspecific localization and even higher than 5 μM shows cytotoxicity determined by vacuole formation and cell detachment (Figure S7). The latter effect is due to the loss of mitochondrial membrane potential upon excess loading of Si-DMA.[39] Hence, in this study, we chose [Si-DMA] less than 100 nM to ensure the homogeneous, selective, and nontoxic staining of mitochondria (Figure 5a,b).

dx.doi.org/10.1021/ja504279r | J. Am. Chem. Soc. 2014, 136, 11707–11715

It is notable that connecting DMA to Si-rhodamine does not affect its intrinsic localization, whereas azo-benzene-substituted Si-rhodamine is mainly localized in the lysosome.[26] Meanwhile, SOSG, a trianionic molecule, stains HeLa cells in a nonspecific and inefficient manner (Figure S2). More importantly, mitochondria are the main target organelles in PDT because mitochondrial actions and dysfunctions are closely related to the programmed cell death.[41−43] Thus, a selective mitochondrial staining of Si-DMA indeed takes advantage of visualizing intracellular $^1O_2$ particularly during PDT.

Fluorescence Detection of Intracellular $^1O_2$: Dependent on the Localization of Sens. To deliver Sens selectively to mitochondria, we chose 5-ALA, which is a commercialized PDT drug as a precursor for the biosynthesis of PpIX.[2,42,44−46] The excess amount of biosynthesized PpIX, which could not be bound to Fe to form heme, is accumulated in mitochondria, and this phenomenon readily happens especially in cancer cells. When the localization of PpIX derived by [5-ALA] = 150 μg mL^{-1} was traced, the synthesized PpIX was found to be initially localized in mitochondria and soon diffused to the cytoplasm (Figure 6a). In particular, PpIX is predominantly localized in

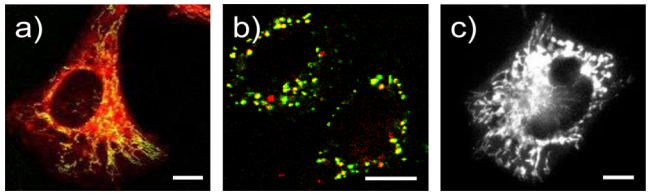

Figure 6. Intracellular localizations of Sens. (a) Fluorescence of MitoTracker Green, 5-ALA-derived PpIX, and merged points are depicted in green, red, and yellow, respectively. (b) Fluorescence of A488-dextran, TMPyP4, and merged points are depicted in green, red, and yellow, respectively. (c) Fluorescence of KillerRed monitored after 24 h transfection of mitochondria-targeted KillerRed vector. Scale bar = 10 μm.

the perinuclear region as reported previously.[42,47,48] In light of the previous reports, 5-ALA was incubated for 4 h in order to maximize the amount of synthesized PpIX (Figure S8).[44,45]

Figure 7a shows reprocessed pseudocolor images of Si-DMA fluorescence in HeLa cells during 640 nm irradiation of PpIX. It is clearly shown that photoirradiation of PpIX induces an increase of Si-DMA fluorescence rapidly (within 10 s) and more significantly in the perinuclear region as compared to the cell edge. The same tendency is observed when the incubation concentration of Si-DMA is increased to 100 nM (Figure S9). Here, an evident fluorescence increase along the mitochondria structure provides a much clearer picture of intracellular $^1O_2$ generation as compared to the previous $^1O_2$ probes with 5-ALA-derived PpIX.[15,17]

It should be confirmed that the fluorescence increase of Si-DMA shown in Figures 7a and S7 is caused by $^1O_2$ generation and not by environmental changes of mitochondria upon PDT. We have monitored approximately 4−6-fold deceleration in the initial rates of fluorescence increase by the addition of a cell-permeable $^1O_2$ quencher, sodium azide (NaN_3) (Figure 8). Furthermore, mitochondrial environmental changes, such as viscosity, did not influence the fluorescence of Si-DMA (Figure S12a).

Subsequently, another type-II Sens that exhibits non-mitochondrial localization is introduced to monitor fluorescence response of Si-DMA. TMPyP4 is one of the frequently used type-II Sens in a model study of PDT because it is water-soluble and can bind to a DNA aptamer, finally delivered to the nucleus of cancer cells.[49−51] Prior to coincubating with Si-DMA, we confirm that TMPyP4 first resides in lysosomes after 24 h incubation (Figure 6b). Next, 640 nm irradiation triggers lysosomal rupture, followed by relocalizations of TMPyP4 to the cytoplasm and nucleus (Figure S10). Relocalization of Sens in lysosomes is a well-known phenomenon in PDT, which maximizes a cytotoxic effect of $^1O_2$ from dispersed Sens molecules.[43,52]

Since fluorescence of TMPyP4 is not intense enough (Φ_{fl} = 0.047 in H_2O)[53] and Q-band absorbance at 640 nm is relatively small, lysosomal rupture events cannot be monitored by TMPyP4 fluorescence with the same photoirradiation and detection conditions used to image Si-DMA. Thus, we additionally stained lysosomes using A647-dextran to observe intracellular events and fluorescence changes of Si-DMA simultaneously with the excitation of TMPyP4. As depicted by the white arrows in Figure 7b, lysosomes containing A647-dextran and TMPyP4 are distinguishable due to their granular structures and strong fluorescence. Upon 640 nm irradiation for 10 s, lysosomal rupture and TMPyP4 diffusion substantially occur. However, fluorescence of Si-DMA does not increase even after TMPyP4 relocalization (Figures 7b and S9).

In short, the heterogeneous fluorescence increase shown in Figure 7a is considered to reflect the localization of PpIX because Si-DMA is localized in mitochondria almost homogeneously over the cell body (Figure 5). In contrast, Si-DMA does not react with $^1O_2$ generated by TMPyP4 (Figure 7b), which changes its location from lysosome to cytoplasm and nucleus upon photoirradiation (Figure S10). Taken together, Si-DMA can respond to only mitochondrial-originating $^1O_2$. This is because of the short diffusion distance of intracellular $^1O_2$ (at longest, approximately 300 nm) in aqueous solution.[9]

Fluorescence Detection of Intracellular $^1O_2$: Dependent on the Type of Sens. We investigated Si-DMA responses depending on the type of Sens. In the previous section, 5-ALA-derived PpIX and TMPyP4 were used, and both are standard type-II Sens with high Φ_Δ (0.54 and 0.74, respectively).[34] As a comparison, KillerRed was chosen as an exemplary case of photosensitizing protein, and it could be expressed selectively in mitochondria (Figure 6c).[54] Upon photoirradiation, the chromophore of KillerRed, the *N*-acylimine group composed of Gln-Tyr-Gly, is excited and subsequently quenched by one-electron reduction from the adjacent amino acid residue, resulting in the radical anion of the chromophore (type-I photosensitization). Its characteristic phototoxicity originates from the presence of a water-filled channel reaching the chromophore of KillerRed.[55,56] Thus, KillerRed can generate a superoxide anion by electron transfer from the radical anion of its chromophore to $^3O_2$.

Pseudocolor images of Si-DMA and KillerRed fluorescence (λ_{em} = 610 nm),[54] collected by the same detection channel (655−725 nm), are shown in Figure 7c. Since λ_{abs} of KillerRed is 585 nm,[54] two-color excitation at 532 and 640 nm is used to excite KillerRed and Si-DMA, respectively. In fact, KillerRed fluorescence is not negligible compared to that of Si-DMA (red spots in the 0 s image of Figure 7c). During 10 min photoirradiation, however, only photobleaching of both species was observed without fluorescence increase of Si-DMA (Figures 7c and S9). As shown in Figure 3, Si-DMA can only respond to $^1O_2$ but not superoxide, hydrogen peroxide, and other ROS. Thus, this result implies that the amount of $^1O_2$

dx.doi.org/10.1021/ja504279r | J. Am. Chem. Soc. 2014, 136, 11707−11715

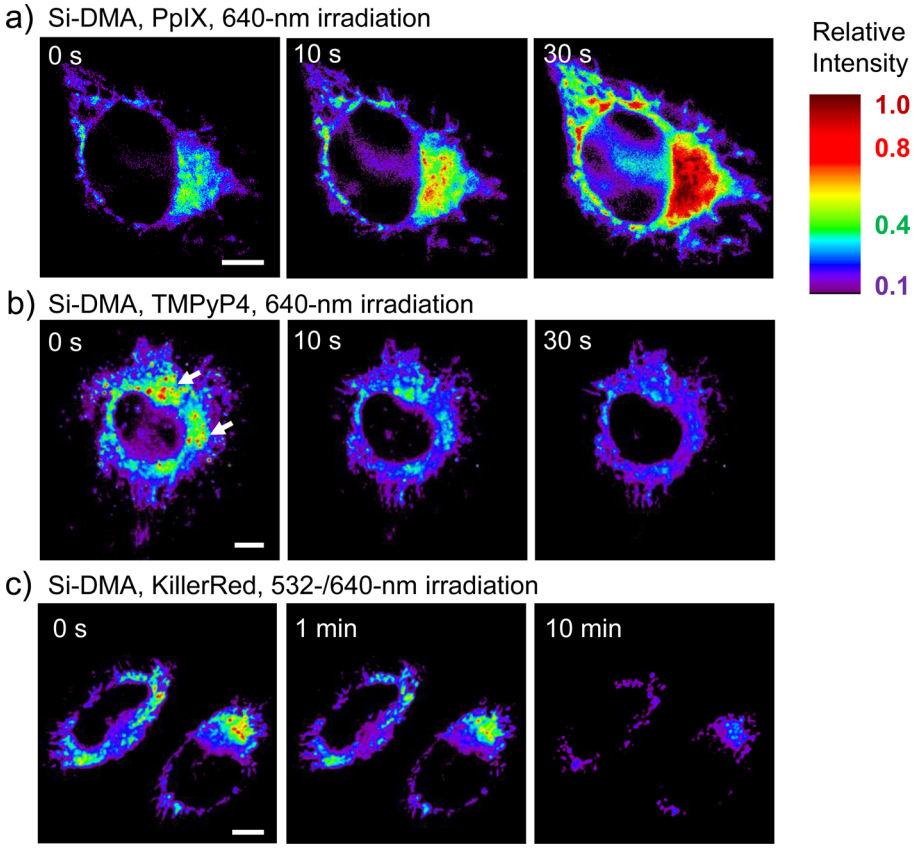

Figure 7. Pseudocolor fluorescence images of HeLa cells with Si-DMA and (a) 5-ALA-induced PpIX, (b) 24 h incubated TMPyP4 and lysosome marker (A647-dextran), and (c) mitochondria-targeted KillerRed. Granular structures indicated by white arrows in (b) are lysosomes that are rapidly ruptured by TMPyP4 irradiation. [Si-DMA] = 25 nM was incubated for 1 h in the HeLa cells containing corresponding Sens. (a,b) One-color irradiation at 640 nm (0.6 W cm^{-2}) was used to generate $^1O_2$ and monitor Si-DMA fluorescence simultaneously. Meanwhile, two-color irradiation was required to excite Si-DMA and KillerRed (c); 0.5 and 0.6 W cm^{-2} were used for 532 and 640 nm irradiation, respectively. Scale bar = 10 μm.

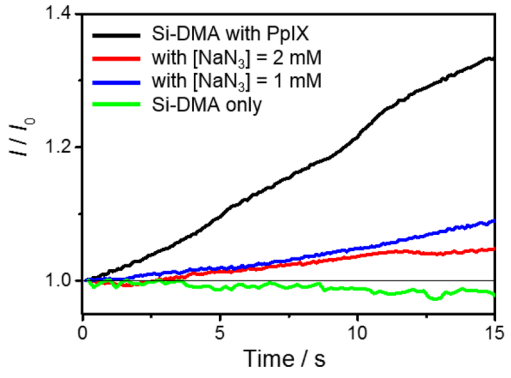

Figure 8. Fluorescence changes of Si-DMA during 15 s of 640 nm irradiation at 0.6 W cm^{-2} with PpIX induced by 5-ALA (black), with the addition of [NaN_3] = 2 mM (red), 1 mM (blue), and Si-DMA without Sens and NaN_3 (green). All data are obtained by averaging mean count changes monitored in 5−8 cells.

generated by KillerRed is far insufficient to induce a conversion of Si-DMA to Si-DMEP even though KillerRed is colocalized in mitochondria. On the other hand, photoirradiation of KillerRed causes relocalization and DNA binding of CellROX Green, which infers the generation of oxygen radical species (Figure S13). Generation of a superoxide anion in a proportional manner upon photoirradiation of KillerRed is in good accord with the previous report.[57]

$^1O_2$ Diffusion Distance and Its Concentration Affect Fluorescence Increase of Si-DMA. To understand different responses of Si-DMA to three Sens (Figure 7), we first considered the total cumulative [$^1O_2$] during photoirradiation of Sens. The extent of PDT cytotoxic effects, so-called PDT dose, is influenced by three factors: light, oxygen, and drug.[7] Here, we used the same light intensity of 640 nm irradiation (except KillerRed), and there is only a slight difference in Q-band absorbance of PpIX and TMPyP4. Furthermore, the previous study found merely a marginal difference of ΔpO_2 between mitochondria or endosomes and air-saturated medium in HeLa cells.[44,58] Overall, nearly identical light doses and homogeneous pO_2 over a whole cell infer that light dose and [$^3O_2$] are not conclusive factors to derive the different results in Si-DMA fluorescence, as shown in Figure 7.

Next, we consider the effective area of $^1O_2$ within its lifetime. Time-resolved phosphorescence measurement is the most direct method to study formation and decay of intracellular $^1O_2$.[1,10] Although the reported lifetime of $^1O_2$ varies depending on the experimental conditions (a few tens of nanoseconds to 3 μs),[2,7,9] the longest travel distance of intracellular $^1O_2$ has been reported to be ∼268 nm over a period t of twice its lifetime.[7] Furthermore, a diameter of mitochondria fibril is ∼200−400 nm,[40] and both Si-DMA and accumulated PpIX are considered to be located inside the mitochondrial inner membrane.[39,46] Such a complete colocalization within a diffusible area of $^1O_2$ is regarded as the main reason for a highly localization-selective response of Si-DMA. On the other hand, $^1O_2$ diffusion across

dx.doi.org/10.1021/ja504279r | J. Am. Chem. Soc. 2014, 136, 11707−11715

different intracellular organelles is theoretically impossible as proven by imaging of Si-DMA fluorescence (Figure 7b).

In the case of KillerRed, the inefficient $^1O_2$ generation of KillerRed is proven by its photocytotoxicity that is rather higher in H_2O than in D_2O[59] and silence at 1270 nm upon photoirradiaiton where $^1O_2$ phosphorescence can be observed.[57] Instead, hydrogen peroxide and a superoxide anion can form $^1O_2$ as a byproduct of the Haber−Weiss reaction (i.e., $H_2O_2 + O_2^{\bullet-} \rightarrow {}^1O_2 + {}^{\bullet}OH + {}^{-}OH$). Vegh et al., however, reported that KillerRed exhibits the quantum yield of hydrogen peroxide generation less than 1% because the generated superoxide anion is quenched inside of the protein by amino acid residues.[57] In fact, even if the superoxide anion is largely generated in a living cell, various enzymatic systems such as superoxide dismutase will quench superoxide to $^3O_2$.[5,6] In accordance with this result, we could not monitor the fluorescence increase of Si-DMA under excessive ROS generation in mitochondria induced by an oxidative burst in RAW 264.7 macrophage (Figure S12c; the detailed discussion can be found in Supporting Information). This finding further supports that Si-DMA maintains its high selectivity to $^1O_2$ in a living cell, while it does not respond to the trace amount of intracellular $^1O_2$. Obtained results in this study are summarized in Table 1.

Table 1. Summary of Si-DMA Responses to Intracellular $^1O_2$ in the Four Experimental Designs

entry	mitochondrial origin of $^1O_2$?	$^1O_2$ generation mechanism	Si-DMA fluorescence
PpIX	yes	TTEnT[a]	increase
TMPyP4	no	TTEnT[a]	no change
KillerRed	yes	electron transfer	no change
oxidative burst	yes	catalytic reaction[4,8]	no change

[a]TTEnT: triplet−triplet intermolecular energy transfer.

Potential Usages of Si-DMA. To conclude, other potential usages of Si-DMA are proposed in addition to visualization of mitochondrial $^1O_2$ during PDT. Using a newly designed far-red fluorescence probe, Si-DMA, we succeeded in increasing the spatial resolution of $^1O_2$ detection up to a single mitochondrial tubule (Figure 7a). This fluorescence increase was never monitored in the case of TMPyP4 that resides in lysosomes, nucleus, and cytoplasm. Considering this highly localization-selective response, we first suggest that Si-DMA can be used as mitochondrial markers of Sens to confirm its accurate internalization. As mentioned above, mitochondria is the main target organelle in the PDT study because dysfunction of mitochondria exerts the strongest cytotoxicity.[41−43] Practically, an infinitesimal addition of Si-DMA to the culture media can quickly stain mitochondria (cf. [Si-DMA] = 20 nM and 30 min incubation was enough to stain). So far, R123 and other cationic dyes have been used to visualize changes in the mitochondrial structure and to confirm localization of a particular substance in mitochondria. In addition to both usages, Si-DMA can further provide information about whether the mitochondria-targeted type-II Sens works properly in terms of $^1O_2$ generation.

Second, Si-DMA can be presumably used to indicate PDT dose and cell viability. Upon prolonged photoirradiation at 640 nm (2−4 min), we could observe fragmentation of the mitochondrial structure and cell shrinkage accompanied by dimmer fluorescence of Si-DMA (Figure S14). Simultaneously, vacuole formation and granular appearance of cell structures were monitored (data are not shown here but are identical to Figure 1 of ref 48). Moreover, fluorescence of Si-DMA upon photoirradiation rarely increased in dying or dead cells. This is considered to be due to (1) defocusing caused by cell morphology change, (2) leak of Si-DMA upon a loss of mitochondrial membrane potential,[48] and (3) increase in overall intracellular viscosity, making a collision between $^1O_2$ and Si-DMA difficult.[60] In this sense, slight fluorescence decrease of Si-DMA shown in Figure 7b (Sens: TMPyP4) is not caused by $^1O_2$-derived photo-oxidation but rather by intracellular environmental change as described above. With further systematic and quantitative studies on the correlation among the fluorescence change of Si-DMA, PDT dose, and cell death pathways (e.g., apoptosis and necrosis), Si-DMA will possibly work as a barometer to report acute cytotoxicity and cell viability during PDT.

CONCLUSION

In this study, we have proposed a new and promising far-red fluorescent probe, Si-DMA, for the intracellular $^1O_2$ detection. As a dyad of Si-rhodamine and DMA, Si-DMA is present as a monomer and H-aggregates in organic solvents and neutral buffered solutions, respectively, while both of the states can react with $^1O_2$. A cationic charge and adequate lipophilicity of Si-DMA facilitate the selective mitochondrial localization. In the cell experiment, fluorescence of Si-DMA increases only by photoirradiation of colocalized and type-II Sens, PpIX. On the other hand, type-II Sens with non-mitochondrial localizations, mitochondria-targeted KillerRed, and an oxidative burst of the macrophage fails to change Si-DMA fluorescence (Table 1). This result confirms a short diffusion distance of $^1O_2$ and substantial generation of $^1O_2$ by type-II Sens (Φ_Δ of PpIX = 0.54). This is the first example of a $^1O_2$ fluorescence probe to suggest a clear image of $^1O_2$ formation during PDT at the subcellular level. To conclude, we would like to emphasize the potential of Si-rhodamine derivatives to be exploited in the single-molecule imaging of intracellular $^1O_2$ during PDT. Unfortunately Si-DMA exhibits a limitation in this application because of its dim fluorescence before reacting to $^1O_2$. Prospective candidates of the new $^1O_2$ probe are required to exhibit a completely dark initial state, enough brightness (extinction coefficient >50 000 M^{-1} cm^{-1}; Φ_{fl} > 0.1),[61] good cell permeability, and water solubility.

ASSOCIATED CONTENT

Supporting Information

Experimental and synthesis details including dye staining, KillerRed expression, ^1H NMR and mass spectrum of Si-DMA, and supporting figures. This material is available free of charge via the Internet at http://pubs.acs.org.

AUTHOR INFORMATION

Corresponding Author

majima@sanken.osaka-u.ac.jp

Notes

The authors declare no competing financial interest.

ACKNOWLEDGMENTS

We are grateful to Prof. A. Sugimoto (SANKEN, Osaka University) for helpful advice on chemical synthesis, and Prof.

T. Kinoshita and Prof. Y. Maeda (iFReC, Osaka University) for help with establishing the biological experimental setup. Also, we acknowledge Prof. W.E. Moerner (Stanford University), Prof. T. Nishi (SANKEN, Osaka University), Dr. M. Morita (Kyoto University), and Dr. J. Seong (iFReC, Osaka University) for fruitful discussions. This work has been partly supported by the Innovative Project for Advanced Instruments, Renovation Center of Instruments for Science Education and Technology, Osaka University, and a Grant-in-Aid for Scientific Research (Projects 25220806, 25288035, and others) from the Ministry of Education, Culture, Sports, Science and Technology (MEXT) of the Japanese Government.

REFERENCES

(1) Ogilby, P. R. *Chem. Soc. Rev.* **2010**, *39*, 3181.
(2) *Advances in Photodynamic Therapy: Basic, Translational, and Clinical*; Hamblin, M. R., Mróz, P., Eds.; Artech House Engineering in Medicine & Biology Series; Artech House: Boston, 2008.
(3) Castano, A. P.; Mroz, P.; Hamblin, M. R. *Nat. Rev. Cancer* **2006**, *6*, 535.
(4) Kanofsky, J. R. *Chem.−Biol. Interact.* **1989**, *70*, 1.
(5) Winterbourn, C. C. *Nat. Chem. Biol.* **2008**, *4*, 278.
(6) Dixon, S. J.; Stockwell, B. R. *Nat. Chem. Biol.* **2014**, *10*, 9.
(7) Jarvi, M. T.; Niedre, M. J.; Patterson, M. S.; Wilson, B. C. *Photochem. Photobiol.* **2006**, *82*, 1198.
(8) Kanofsky, J. R.; Hoogland, H.; Wever, R.; Weiss, S. J. *J. Biol. Chem.* **1988**, *263*, 9692.
(9) Skovsen, E.; Snyder, J. W.; Lambert, J. D. C.; Ogilby, P. R. *J. Phys. Chem. B* **2005**, *109*, 8570.
(10) Celli, J. P.; Spring, B. Q.; Rizvi, I.; Evans, C. L.; Samkoe, K. S.; Verma, S.; Pogue, B. W.; Hasan, T. *Chem. Rev.* **2010**, *110*, 2795.
(11) Snyder, J. W.; Skovsen, E.; Lambert, J. D. C.; Poulsen, L.; Ogilby, P. R. *Phys. Chem. Chem. Phys.* **2006**, *8*, 4280.
(12) Tanaka, K.; Miura, T.; Umezawa, N.; Urano, Y.; Kikuchi, K.; Higuchi, T.; Nagano, T. *J. Am. Chem. Soc.* **2001**, *123*, 2530.
(13) Liu, Y.-J.; Wang, K.-Z. *Eur. J. Inorg. Chem.* **2008**, *2008*, 5214.
(14) Ruiz-González, R.; Zanocco, R.; Gidi, Y.; Zanocco, A. L.; Nonell, S.; Lemp, E. *Photochem. Photobiol.* **2013**, *89*, 1427.
(15) Pedersen, S. K.; Holmehave, J.; Blaikie, F. H.; Gollmer, A.; Breitenbach, T.; Jensen, H. H.; Ogilby, P. R. *J. Org. Chem.* **2014**, *79*, 3079.
(16) Song, B.; Wang, G.; Tan, M.; Yuan, J. *J. Am. Chem. Soc.* **2006**, *128*, 13442.
(17) Dai, Z.; Tian, L.; Xiao, Y.; Ye, Z.; Zhang, R.; Yuan, J. *J. Mater. Chem. B* **2013**, *1*, 924.
(18) Xu, K.; Wang, L.; Qiang, M.; Wang, L.; Li, P.; Tang, B. *Chem. Commun.* **2011**, *47*, 7386.
(19) Song, D.; Cho, S.; Han, Y.; You, Y.; Nam, W. *Org. Lett.* **2013**, *15*, 3582.
(20) Oliveira, M. S.; Severino, D.; Prado, F. M.; Angeli, J. P. F.; Motta, F. D.; Baptista, M. S.; Medeiros, M. H. G.; Di Mascio, P. *Photochem. Photobiol. Sci.* **2011**, *10*, 1546.
(21) Gollmer, A.; Arnbjerg, J.; Blaikie, F.; Pedersen, B.; Breitenbach, T.; Daasbjerg, K.; Glasius, M.; Ogilby, P. *Photochem. Photobiol.* **2011**, *87*, 671.
(22) Kim, S.; Fujitsuka, M.; Majima, T. *J. Phys. Chem. B* **2013**, *117*, 13985.
(23) Koide, Y.; Urano, Y.; Hanaoka, K.; Terai, T.; Nagano, T. *ACS Chem. Biol.* **2011**, *6*, 600.
(24) Koide, Y.; Urano, Y.; Hanaoka, K.; Piao, W.; Kusakabe, M.; Saito, N.; Terai, T.; Okabe, T.; Nagano, T. *J. Am. Chem. Soc.* **2012**, *134*, 5029.
(25) Egawa, T.; Hanaoka, K.; Koide, Y.; Ujita, S.; Takahashi, N.; Ikegaya, Y.; Matsuki, N.; Terai, T.; Ueno, T.; Komatsu, T.; Nagano, T. *J. Am. Chem. Soc.* **2011**, *133*, 14157.
(26) Piao, W.; Tsuda, S.; Tanaka, Y.; Maeda, S.; Liu, F.; Takahashi, S.; Kushida, Y.; Komatsu, T.; Ueno, T.; Terai, T.; Nakazawa, T.; Uchiyama, M.; Morokuma, K.; Nagano, T.; Hanaoka, K. *Angew. Chem., Int. Ed.* **2013**, *52*, 13028.
(27) Lukinavičius, G.; Umezawa, K.; Olivier, N.; Honigmann, A.; Yang, G.; Plass, T.; Mueller, V.; Reymond, L.; Corrêa, I. R.; Luo, Z. G.; Schultz, C.; Lemke, E. A.; Heppenstall, P.; Eggeling, C.; Manley, S.; Johnsson, K. *Nat. Chem.* **2013**, *5*, 132.
(28) Miura, T.; Urano, Y.; Tanaka, K.; Nagano, T.; Ohkubo, K.; Fukuzumi, S. *J. Am. Chem. Soc.* **2003**, *125*, 8666.
(29) Fudickar, W.; Linker, T. *J. Am. Chem. Soc.* **2012**, *134*, 15071.
(30) Martinez, V.; Arbeloa, F.; Prieto, J.; Lopez, T.; Arbeloa, I. *J. Phys. Chem. B* **2004**, *108*, 20030.
(31) Nasr, C.; Liu, D.; Hotchandani, S.; Kamat, P. V. *J. Phys. Chem.* **1996**, *100*, 11054.
(32) McCann, T. E.; Kosaka, N.; Koide, Y.; Mitsunaga, M.; Choyke, P. L.; Nagano, T.; Urano, Y.; Kobayashi, H. *Bioconjugate Chem.* **2011**, *22*, 2531.
(33) Ragas, X.; Jimenez-Banzo, A.; Sanchez-Garcia, D.; Batllori, X.; Nonell, S. *Chem. Commun.* **2009**, 2920.
(34) Redmond, R. W.; Gamlin, J. N. *Photochem. Photobiol.* **1999**, *70*, 391.
(35) Johnson, L. V.; Walsh, M. L.; Chen, L. B. *Proc. Natl. Acad. Sci. U.S.A.* **1980**, *77*, 990.
(36) Galluzzi, L.; Zamzami, N.; de la Motte Rouge, T.; Lemaire, C.; Brenner, C.; Kroemer, G. *Apoptosis* **2007**, *12*, 803.
(37) Smiley, S. T.; Reers, M.; Mottola-Hartshorn, C.; Lin, M.; Chen, A.; Smith, T. W.; Steele, G. D.; Chen, L. B. *Proc. Natl. Acad. Sci. U.S.A.* **1991**, *88*, 3671.
(38) Salvioli, S.; Ardizzoni, A.; Franceschi, C.; Cossarizza, A. *FEBS Lett.* **1997**, *411*, 77.
(39) Skulachev, V. P. *Trends Biochem. Sci.* **2001**, *26*, 23.
(40) Schmidt, R.; Wurm, C. A.; Punge, A.; Egner, A.; Jakobs, S.; Hell, S. W. *Nano Lett.* **2009**, *9*, 2508.
(41) Kroemer, G.; Dallaporta, B.; Resche-Rigon, M. *Annu. Rev. Physiol.* **1998**, *60*, 619.
(42) Steinbach, P.; Wedmgandt, H.; Baumgartner, R.; Kriegmair, M.; Hofstädter, F.; Knüchel, R. *Photochem. Photobiol.* **1995**, *62*, 887.
(43) Castano, A. P.; Demidova, T. N.; Hamblin, M. R. *Photodiagn. Photodyn. Ther.* **2004**, *1*, 279.
(44) Mik, E.; Stap, J.; Sinaasappel, M.; Beek, J.; Aten, J.; van Leeuwen, T.; Ince, C. *Nat. Methods* **2006**, *3*, 939.
(45) Atif, M.; Firdous, S.; Khurshid, A.; Noreen, L.; Zaidi, S. S. Z.; Ikram, M. *Laser Phys. Lett.* **2009**, *6*, 886.
(46) Peng, Q.; Berg, K.; Moan, J.; Kongshaug, M.; Nesland, J. M. *Photochem. Photobiol.* **1997**, *65*, 235.
(47) Gaullier, J.-M.; Gèze, M.; Santus, R.; Melo, T. S. E.; Mazière, J.-C.; Bazin, M.; Morlière, P.; Dubertret, L. *Photochem. Photobiol.* **1995**, *62*, 114.
(48) Gollmer, A.; Besostri, F.; Breitenbach, T.; Ogilby, P. R. *Free Radical Res.* **2013**, *47*, 718.
(49) Shieh, Y.-A.; Yang, S.-J.; Wei, M.-F.; Shieh, M.-J. *ACS Nano* **2010**, *4*, 1433.
(50) Yuan, Q.; Wu, Y.; Wang, J.; Lu, D.; Zhao, Z.; Liu, T.; Zhang, X.; Tan, W. *Angew. Chem., Int. Ed.* **2013**, *52*, 13965.
(51) Yin, M.; Li, Z.; Liu, Z.; Ren, J.; Yang, X.; Qu, X. *Chem. Commun.* **2012**, *48*, 6556.
(52) da Silva, E. F. F.; Pedersen, B. W.; Breitenbach, T.; Toftegaard, R.; Kuimova, M. K.; Arnaut, L. G.; Ogilby, P. R. *J. Phys. Chem. B* **2011**, *116*, 445.
(53) Kalyanasundaram, K. *Inorg. Chem.* **1984**, *23*, 2453.
(54) Bulina, M. E.; Lukyanov, K. A.; Britanova, O. V.; Onichtchouk, D.; Lukyanov, S.; Chudakov, D. M. *Nat. Protoc.* **2006**, *1*, 947.
(55) Carpentier, P.; Violot, S.; Blanchoin, L.; Bourgeois, D. *FEBS Lett.* **2009**, *583*, 2839.
(56) Pletnev, S.; Gurskaya, N. G.; Pletneva, N. V.; Lukyanov, K. A.; Chudakov, D. M.; Martynov, V. I.; Popov, V. O.; Kovalchuk, M. V.; Wlodawer, A.; Dauter, Z.; Pletnev, V. *J. Biol. Chem.* **2009**, *284*, 32028.
(57) Vegh, R. B.; Solntsev, K. M.; Kuimova, M. K.; Cho, S.; Liang, Y.; Loo, B. L. W.; Tolbert, L. M.; Bommarius, A. S. *Chem. Commun.* **2011**, *47*, 4887.

(58) Finikova, O. S.; Lebedev, A. Y.; Aprelev, A.; Troxler, T.; Gao, F.; Garnacho, C.; Muro, S.; Hochstrasser, R. M.; Vinogradov, S. A. *ChemPhysChem* **2008**, *9*, 1673.
(59) Serebrovskaya, E. O.; Edelweiss, E. F.; Stremovskiy, O. A.; Lukyanov, K. A.; Chudakov, D. M.; Deyev, S. M. *Proc. Natl. Acad. Sci. U.S.A.* **2009**, *106*, 9221.
(60) Kuimova, M.; Botchway, S.; Parker, A.; Balaz, M.; Collins, H.; Anderson, H.; Suhling, K.; Ogilby, P. *Nat. Chem.* **2009**, *1*, 69.
(61) Roy, R.; Hohng, S.; Ha, T. *Nat. Methods* **2008**, *5*, 507.